Experimental Validation on Connected Cruise Control With Flexible Connectivity Topologies

Wubing B. Qin and Gábor Orosz

***Abstract*—In this paper, we investigate experimentally the impact of connected automated vehicles on the dynamics of vehicle chains with different connectivity topologies. We utilize a scaled connected vehicle testbed consisting of ground robots that can mimic the dynamics of human-driven and connected automated vehicles. We derive analytical conditions for stability and disturbance attenuation (i.e., string stability) while taking into account digital effects and delays and validate the corresponding stability diagrams experimentally. The flexibility and robustness of vehicle-to-everything (V2X) based longitudinal control among human-driven vehicles is evaluated for different connectivity topologies and the impacts of connected automated vehicles on traffic flow are highlighted.**

***Index Terms*—Connected automated vehicles (CAVs), ground robots, string stability, vehicle-to-vehicle (V2V) communication.**

I. Introduction

THE growing numbers of automobiles on the road are resulting increasing level of traffic congestion, leading to increased travel time, growing number of traffic accidents, and more wasted energy [1]. During the last few decades automotive industry has been moving toward enhanced vehicle automation with the primary goal of advancing the safety of road users. These systems may also have a positive impact on traffic congestion once their penetration rate reaches a certain level. However, safety and congestion mitigation may require different control design, and high penetration rate of automated vehicles (AVs) may be needed to have a significant impact. In the meantime, automakers and suppliers are exploring different technologies (WiFi, LTE, 5G) [2] to facilitate V2X communication [3]–[6], which allows vehicles to obtain information from beyond the line of sight. When V2X information is incorporated in the control and decision-making algorithms of AVs, they become CAVs. Then, a key question is whether and how such V2X information can be used to improve the performance of CAVs and the performance of the overall traffic system.

Manuscript received March 2, 2018; revised November 18, 2018 and March 6, 2019; accepted September 16, 2019. Date of publication September 24, 2019; date of current version December 31, 2019. Recommended by Technical Editor D. Cao. This work was supported by National Science Foundation under Grant 1300319. *(Corresponding author: Wubing B. Qin.)*

The authors are with the Department of Mechanical Engineering, University of Michigan, Ann Arbor, MI 48109 USA (e-mail: wubing@umich.edu; orosz@umich.edu).

Color versions of one or more of the figures in this article are available online at http://ieeexplore.ieee.org.

Digital Object Identifier 10.1109/TMECH.2019.2943501

In this paper, we try to answer this question partially, while restricting ourselves to vehicle chains, that is, we focus on designing longitudinal controllers for CAVs. The idea of automating the longitudinal motion of road vehicles that follow each other, dates back a few decades. If all vehicles were AVs, one may expect improvement in safety, fuel economy, driving comfort, and traffic efficiency. Further improvements may be achieved by adding V2V communication to a group of AVs [7] as cooperative control may allow vehicles to have smaller following distances and larger throughput. This is often referred to as cooperative adaptive cruise control [8]–[16] and it is expected to penetrate the trucking industry because of improvements on fuel economy due to reduced air drag [17], [18]. However, humans are expected to dominate traffic systems in the forthcoming decades. One may focus on strategy when CAVs benefit from connectivity without requiring automation of surrounding vehicles. We refer to this strategy as connected cruise control (CCC) and recent theoretical research shows that system level benefits may be obtained even for low penetration rate of CAVs [19]–[24]. However, we are still lacking experimental evidence of these claims.

In order to respond to this challenge we built a scaled connected vehicle testbed consisting of ground robots. The robots are designed to capture the longitudinal and lateral vehicle dynamics and exchange information using wireless peer-to-peer communication. Model-based design allows us to make some of the robots mimic the longitudinal dynamics of human-driven vehicles that amplify velocity fluctuations due to large reaction delays. Other robots play the role of CAVs and run CCC algorithms that allow them to respond to the motion of multiple human-driven vehicles ahead and mitigate the velocity fluctuations effectively. This set up, for the first time, allows for a systematic experimental investigation of the impact of CAVs in human-driven traffic flow. In particular, we study experimentally the mitigation of velocity fluctuations (characterized by head-to-tail string stability) for different penetration rates and different distributions of CAVs while exploring different connectivity topologies. We demonstrate that by utilizing information obtained via V2X connectivity one can significantly increase the benefits provided by automation for traffic.

The remainder of this paper is organized as follows. In Section II, we lay out the performance requirements and design a CCC controller that may utilize all available V2X signals. In Section III, the mechanical structure and the electronic control system of the testbed are explained briefly. In Section IV, a dynamic model is proposed to describe the system, and the stability analysis is performed based on the digital implementation

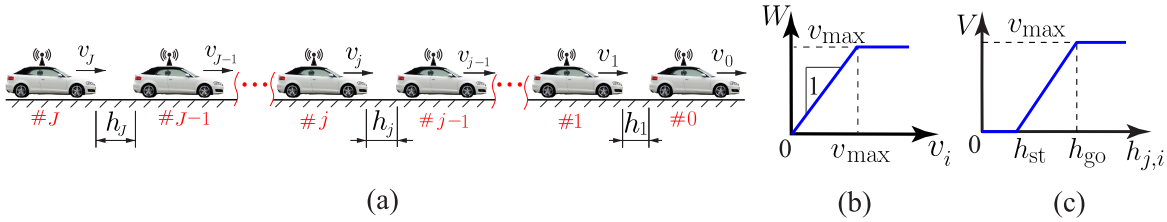

Fig. 1. (a) A chain of connected vehicles. (b) Target velocity (2). (c) Range policy function (3).

of the controller. In Section V, experiments are conducted on the robots with different connectivity topologies to show the benefits of CCC in different traffic scenarios. In Section VI, conclusions are drawn and future research directions are pointed out.

II. Performance Requirements and Controller Design

In this section, we describe the performance requirements for connected vehicle systems and propose a class of connected cruise controllers that can satisfy these requirements. In particular, we focus on plant stability and string stability as well as scalability of the algorithms [21], [25]–[27].

In order to define these requirements, let us consider a chain of connected vehicles labeled as $0, \dots, J$ from the head to the tail as depicted in Fig. 1(a). We say that a vehicle is *plant stable* if, assuming the vehicle ahead is traveling at a constant velocity, it can approach this velocity. Indeed, a vehicle chain is *plant stable* when all the vehicles in this chain are plant stable. Plant instability leads to diverging velocity and may even result in collisions.

String stability refers to attenuation of velocity fluctuations as they propagate backward along the vehicle chain. More precisely, one may compare the motion of two vehicles in the chain and define that the chain is *i- to-j string stable* ($i < j$) when the velocity fluctuations of vehicle i are attenuated when arriving at vehicle j. Note that 0-to-J string stability (often referred to as *head-to-tail string stability*) may be used to characterize the performance of the whole vehicle chain [25]. We remark that i-to-j string stability does not imply that vehicles between i and j attenuate perturbations. This allows us to apply the definition to connected vehicle systems containing human-driven vehicles whose motion cannot be designed. As a matter of fact, humans typically amplify velocity fluctuations when responding to the motion of preceding vehicle due to limited perception abilities and large reaction time. That is, they are $(j-1)$-to-j string unstable (often simply referred to as string unstable). Still, by equipping the j-th vehicle with connected cruise controller that utilizes motion information from multiple vehicles ahead, it may achieve i-to-j string stability when human-driven vehicles are included in between.

In order to achieve plant stability and head-to-tail string stability, the CCC vehicle may utilize the position and velocity information of the vehicles ahead that are equipped with V2X devices. In Fig. 1(a), v_j represents the j-th vehicle's velocity, and h_j is the intervehicle distance between vehicle $j-1$ and j, called *distance headway*. The controller of the CCC vehicle j may try to match its velocity v_j with the preceding vehicles' velocities v_i for $i = 0, \dots, j-1$, and also regulate the average distance headway

$$h_{j,i} = \frac{1}{j-i} \sum_{l=i+1}^{j} h_l \tag{1}$$

between vehicle j and vehicle i.

When velocity v_i exceeds the speed limit $v_j^{\max}$, the controller should not try to match the velocity v_i but rather keep $v_j^{\max}$. That is, the target velocity can be formulated as

$$W_j(v_i) = \begin{cases} v_i & \text{if } \ v_i < v_j^{\max} \\ v_j^{\max} & \text{if } \ v_i \geq v_j^{\max} \end{cases} \tag{2}$$

shown in Fig. 1(b).

The distance regulatory mechanism typically involves a *range policy*, which provides the desired velocity V_j at the given distance headway $h_{j,i}$. Different range policies can be considered, but they must be:

1) continuous and monotonously increasing (the more sparse traffic is, the faster vehicles intend to run);
2) zero for $h_{j,i} \leq h_j^{\text{st}}$ (vehicles intend to stop within a safety distance);
3) maximal for $h_{j,i} \geq h_j^{\text{go}}$ (vehicles intend to run with a given maximum speed in sparse traffic—often referred to as *free flow*).

Here, we choose

$$V_j(h_{j,i}) = \begin{cases} 0 & \text{if } \ h_{j,i} \leq h_j^{\text{st}} \\ \dfrac{v_j^{\max}}{h_j^{\text{go}} - h_j^{\text{st}}} \left(h_{j,i} - h_j^{\text{st}}\right) & \text{if } \ h_j^{\text{st}} < h_{j,i} < h_j^{\text{go}} \\ v_j^{\max} & \text{if } \ h_{j,i} \geq h_j^{\text{go}} \end{cases} \tag{3}$$

depicted in Fig. 1(c). The reciprocal of the slope of the linear segment

$$t_j^{\text{h}} = \frac{h_j^{\text{go}} - h_j^{\text{st}}}{v_j^{\max}} \tag{4}$$

is often referred to as *time headway*.

In order to match velocities and regulate distance headway, we propose the CCC controller

$$\begin{aligned} u_j &= \sum_{i=0}^{j-1} \left(\alpha_{j,i}\big(V_j(h_{j,i}) - v_j\big) + \beta_{j,i}\big(W_j(v_i) - v_j\big)\right) + \gamma_j\, \varepsilon_j \\ \dot{\varepsilon}_j &= V_j(h_j) - v_j \end{aligned} \tag{5}$$

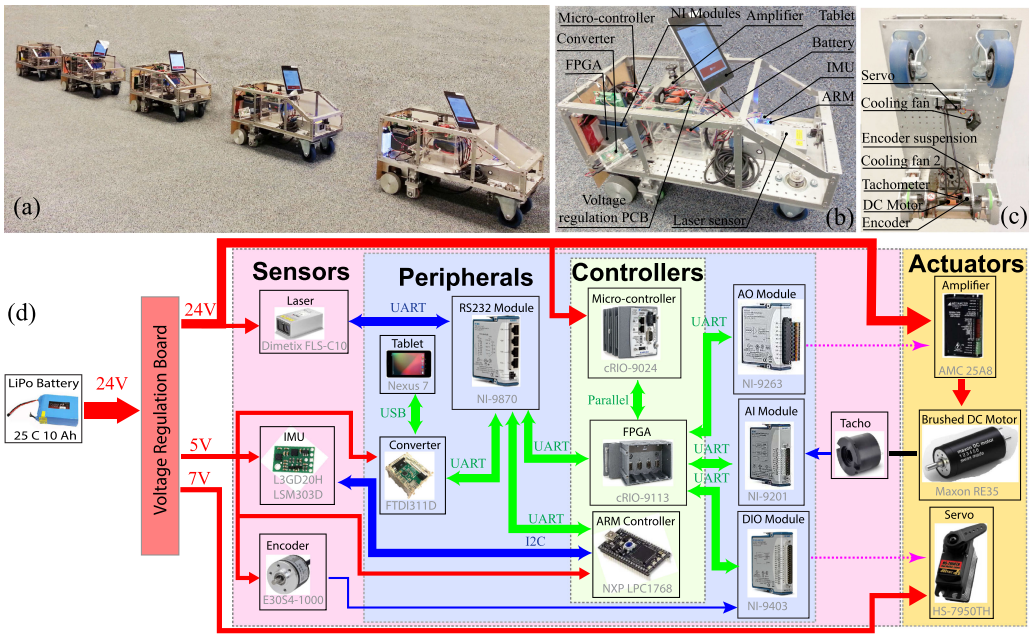

Fig. 2. (a) The testbed of ground robots. (b) Side view of a robot and accessories. (c) Bottom view of a robot. (d) Functional block diagram of the robots.

where u_j is the commanded acceleration. The term $V_j(h_{j,i}) - v_j$ represents the error between the desired velocity $V_j(h_{j,i})$ and the vehicle's velocity v_j, $W_j(v_i) - v_j$ represents the velocity matching error, and the integrator is used to eliminate steady-state error. We remark that although the errors that regulate the average distance $h_{j,i}$ contribute to the control command u_j to achieve fast responses to upcoming traffic, the intervehicle distance h_j is governed by the velocity of its preceding vehicle through the integral term. Note that $\alpha_{j,i}$ and $\beta_{j,i}$ are measured in $[1/\mathrm{s}]$, γ_j is measured in $[1/\mathrm{s}^2]$. Also, $\alpha_{j,i}$ and $\beta_{j,i}$ are zeros when vehicle i does not communicate or the motion of vehicle i is not utilized in the controller of vehicle j.

In the rest of this paper, we will analyze CCC controllers of the form (5) both theoretically and experimentally with different connectivity topologies and penetration rates. Specifically, plant stability and head-to-tail string stability are the key performance index. We remark that the controller (5) should be able to avoid collision if plant stability and head-to-tail string stability are satisfied. However, future research will provide more rigorous proof, and one can refer to [28] for reference. We will demonstrate that appropriately designed CCC may improve the performance of traffic systems.

III. Testbed Setup

In order to test the proposed controller (5), we utilize a group of ground robots shown in Fig. 2(a) to mimic the longitudinal dynamics of real vehicles. In this section, we briefly explain the mechanical structure and the electronic control system of the robots.

The mechanical components and structure of a robot are shown in Fig. 2(b) and (c). During the design process, length and time are scaled by $1/8$ and 2, respectively, such that the similitude theory holds and the experimental results on the robots can provide us with insights on the performance of real vehicles; see Appendix B for similarity verification. All the other derived scaling factors are shown in Table I, while Table II shows the control parameters used in the controller (5) based on the scaling.

TABLE I
Scaling Factors From Real Vehicles to Robots

length [m]	$1/8$
time [s]	2
velocity [m/s]	$1/16$
frequency [Hz]	$1/2$
acceleration [m/s^2]	$1/32$
control gains $\alpha_{j,i}$ [1/s]	1/2
control gains $\beta_{j,i}$ [1/s]	1/2
control gains γ_j [1/s^2]	1/4

TABLE II
Control Parameters Used in the Experiments

	Real Vehicles	Robots
$v_j^{\max}$ [m/s]	30	1.875
h_j^{st} [m]	5	0.625
h_j^{go} [m]	35	4.375
t_j^{h} [s]	1	2

Fig. 2(d) shows the functional block diagram of a robot's electronic control system, composed of power system, sensors, actuators, controllers, and peripherals. Each robot is made aware of its position, velocity, acceleration, and yaw rate with the help of a laser range sensor, two optical encoders, a tachometer, and an inertial measurement unit (IMU). Each robot is rear-wheel driven by a brushed direct current (DC) motor and front-wheel steered by a servo motor. A servo amplifier working in current mode is used to amplify the control signals that drive the DC motor, such that the motor torque tracks the commanded torque.

TABLE III
PHYSICAL PARAMETERS OF THE ROBOTS

mass of the robot m [kg]	20.2
rear wheel radius R [m]	0.045
gear ratio η	55/18
air drag coefficient ν [kg/m]	0 (neglected)
damping ratio b [kg/s]	0 (neglected)
rolling resistance coefficient μ	0.008

The higher-level controller and data logging are implemented on an 800 MHz microcontroller, while a field programmable gate array (FPGA) and an advance reduced instruction set computer (RISC) machine (ARM) are used to preprocess data and communicate with peripherals via different interfaces. Among the peripherals, an important component is an android tablet that allows robots to establish wireless peer-to-peer communication with each other, that is, they mimic V2X devices. Moreover, the tablets also serve as human–machine interfaces.

IV. MODELING AND ANALYSIS

In this section, we model the longitudinal vehicle dynamics of the robots and derive the closed-loop dynamics while using the digital implementation of controller (5). Then, linearization and discretization are used to carry out stability analysis, and plant stability and string stability conditions are derived in order to guide the forthcoming experiments.

A. Dynamics

To model the longitudinal dynamics, we consider no slip on the wheels and neglect flexibility of the tires and the suspension that results in the differential equation

$$m_{\text{eff}}\,\dot{v}_j = -mg\sin\phi - \mu\, mg\cos\phi - b\,v_j - \nu(v_j+v_{\text{w}})^2 + \frac{\eta\, T_j}{R} \tag{6}$$

where $m_{\text{eff}} = m + J/R^2$ is the effective mass, containing the mass of the vehicle m, the moment of inertia J of the rotating elements, and the wheel radius R. Also, g is the gravitational constant, ϕ is the inclination angle, μ is the rolling resistance coefficient, b is the damping ratio, ν is the air drag constant, v_{w} is the velocity of the head wind, η is the gear ratio, and T_j is the motor torque; see Table III.

To simplify the analysis, we assume no elevation ($\phi = 0$) and no head wind ($v_{\text{w}} = 0$). In addition, we neglect the moment of inertia of the rotational parts ($J = 0$ implying $m_{\text{eff}} = m$). Using the intervehicle distance h_j and the speed v_j as state variables we obtain

$$\begin{aligned}\dot{h}_j &= v_{j-1} - v_j\\ \dot{v}_j &= -\mu\, g - \frac{b}{m}v_j - \frac{\nu}{m}v_j^2 + \frac{\eta\, T_j}{mR}\end{aligned} \tag{7}$$

and the torque command

$$T_j = \frac{mR}{\eta}\left(u_j + \bar{\mu}\, g + \frac{\bar{b}}{m}v_j + \frac{\bar{\nu}}{m}v_j^2\right) \tag{8}$$

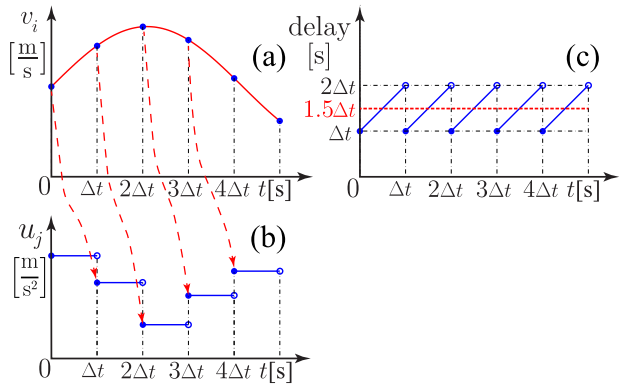

Fig. 3. (a) Velocity sampling. (b) Digital control. (c) Delay variations.

consists of the feedback controller u_j in (5) and three feedforward terms to compensate resistance based on nominal rolling resistance coefficient $\bar{\mu}$, nominal damping ratio $\bar{b}$, and nominal air drag constant $\bar{\nu}$.

We synchronize the clocks among vehicles and their kinematic information is sampled with period Δt, resulting in the time mesh $t_k = k\Delta t$, $k = 0, 1, 2, \ldots$, see Fig. 3(a). The collected information is broadcast according to a scheduling algorithm [24] ensuring that the messages are received and processed within Δt time. Thus, when no packets are lost in V2V communication, the information available to vehicle j at time instant t_k is the state of other vehicles at time t_{k-1}. Based on this information, the digital controller on vehicle j outputs an actuation command at t_k that is held constant until t_{k+1} using *zero-order-hold*, see Fig. 3(b). This means that the effective delay increases from Δt to $2\,\Delta t$ during each control interval as shown in Fig. 3(c), resulting in the average delay $1.5\,\Delta t$. Note that the physical system still evolves in continuous time while subject to digital control, that is,

$$\begin{aligned}\dot{h}_j &= v_{j-1} - v_j\\ \dot{v}_j &= -\tilde{\mu}\, g - \frac{\tilde{b}}{m}v_j - \frac{\tilde{\nu}}{m}v_j^2\\ &\quad + \sum_{i=0}^{j-1}\left(\alpha_{j,i}\left(V_j\left(h_{j,i}(t_{k-1})\right) - v_j(t_{k-1})\right)\right.\\ &\quad \left. + \beta_{j,i}\left(W_j\left(v_i(t_{k-1})\right) - v_j(t_{k-1})\right)\right) + \gamma_j\,\varepsilon_j(t_k)\\ \varepsilon_j(t_k) &= \varepsilon_j(t_{k-1}) + \left(V_j\left(h_j(t_{k-1})\right) - v_j(t_{k-1})\right)\Delta t\end{aligned} \tag{9}$$

for $j = 1, \ldots, J$ when $t \in [t_k,\, t_{k+1})$. Here

$$\tilde{\mu} = \mu - \bar{\mu}\,, \qquad \tilde{b} = b - \bar{b}\,, \qquad \tilde{\nu} = \nu - \bar{\nu} \tag{10}$$

are the errors between real values and the corresponding nominal values.

When the velocities do not exceed the speed limit, system (9) possesses the equilibrium

$$\begin{aligned}v_j^* &= V_j(h_j^*) = v_0^*\\ \varepsilon_j^* &= \frac{1}{\gamma_j}\left(\tilde{\mu}\, g + \frac{\tilde{b}}{m}v_j^* + \frac{\tilde{\nu}}{m}(v_j^*)^2\right)\end{aligned} \tag{11}$$

for $j = 1, \ldots, J$, where vehicles travel with the same velocity as the head vehicle while maintaining safety distance given by their own range policy. This is often referred to as the *uniform flow equilibrium*.

We linearize the system about the equilibrium (11) and discretize the obtained linear equations. Using the perturbations

$$\tilde{h}_j = h_j - h_j^*, \qquad \tilde{v}_j = v_j - v_j^*, \qquad \tilde{\varepsilon}_j = \varepsilon_j - \varepsilon_j^* \tag{12}$$

one may obtain

$$\dot{\tilde{h}}_j = \tilde{v}_{j-1} - \tilde{v}_j \tag{13}$$

$$\begin{aligned}\dot{\tilde{v}}_j = \; & -c\,\tilde{v}_j + \sum_{i=0}^{j-1} \left(\frac{\alpha_{j,i}}{t_j^{\mathrm{h}}} \cdot \frac{1}{j-i} \sum_{l=i+1}^{j} \tilde{h}_l(k-1) \right. \\ & \left. + \beta_{j,i}\tilde{v}_i(k-1) - (\alpha_{j,i}+\beta_{j,i})\,\tilde{v}_j(k-1) \right) + \gamma_j\,\tilde{\varepsilon}_j(k)\end{aligned} \tag{14}$$

$$\tilde{\varepsilon}_j(k) = \tilde{\varepsilon}_j(k-1) + \frac{\Delta t}{t_j^{\mathrm{h}}}\,\tilde{h}_j(k-1) - \Delta t\,\tilde{v}_j(k-1) \tag{15}$$

for $j = 1, \ldots, J$ when $t \in [t_k, t_{k+1})$. Here, we used the lumped constant

$$c = \frac{\tilde{b} + 2\,\tilde{\nu}\,v^*}{m} \tag{16}$$

and introduced the shorthand notation $\tilde{h}_j(k) = \tilde{h}_j(t_k)$, $\tilde{v}_j(k) = \tilde{v}_j(t_k)$, and $\tilde{\varepsilon}_j(k) = \tilde{\varepsilon}_j(t_k)$, while $\tilde{h}_j$, $\tilde{v}_j$, $\tilde{\varepsilon}_j$, and $\tilde{v}_{j-1}$ without arguments represent continuous-time variables.

Based on Fourier theory, a periodic signal can be represented as a countable sum of sines and cosines, which can also be extended to absolutely integrable nonperiodic signals using Fourier transform. Henceforth, assuming sinusoidal variations in the head vehicle's velocity, i.e.,

$$v_0(t) = v_0^* + v_0^{\mathrm{amp}} \sin(\omega\,t) \implies \tilde{v}_0(t) = v_0^{\mathrm{amp}} \sin(\omega\,t) \tag{17}$$

and solving the system (13,14,15) from t_k to t_{k+1}, one can obtain

$$X_j(k+1) = \sum_{l=1}^{j} \mathbf{A}_{j,l}\,X_l(k) + \mathbf{B}_j\,U(k) \tag{18}$$

for $j = 1, \ldots, J$, where the state and the input are given by

$$X_j(k) = \begin{bmatrix} \tilde{h}_j(k) \\ \tilde{v}_j(k) \\ \tilde{\varepsilon}_j(k) \\ \tilde{h}_j(k-1) \\ \tilde{v}_j(k-1) \end{bmatrix}, \qquad U(k) = \begin{bmatrix} \tilde{v}_0(k) \\ \tilde{v}_0^{\perp}(k) \end{bmatrix} \tag{19}$$

with

$$\tilde{v}_0^{\perp}(t) = v_0^{\mathrm{amp}} \cos(\omega\,t)\,. \tag{20}$$

The derivations and matrices $\mathbf{A}_{j,l}$ and $\mathbf{B}_j$ are provided in (38)–(41) in Appendix A. Notice that the scalar sinusoidal input (17) for the continuous-time system (9) results in the vector-valued input (19) for the discrete-time system (18) (though the two components are dependent).

We remark that there exist many methods [29] to convert a continuous-time system with digital controllers to a discrete-time system and then derive head-to-tail transfer function from (18). The following way is used to facilitate the understanding of connectivity structure. We rewrite the overall system as

$$\begin{aligned} X(k+1) &= \mathbf{A}X(k) + \mathbf{B}\,U(k) \\ Y(k) &= \mathbf{C}X(k) \end{aligned} \tag{21}$$

where the state and the output are given by

$$X(k) = \begin{bmatrix} X_1(k) \\ X_2(k) \\ \vdots \\ X_J(k) \end{bmatrix}, \qquad Y(k) = \tilde{v}_J(k) \tag{22}$$

and the matrices are

$$\mathbf{A} = \begin{bmatrix} \mathbf{A}_{1,1} & & & \\ \mathbf{A}_{2,1} & \mathbf{A}_{2,2} & & \\ \vdots & \ddots & \ddots & \\ \mathbf{A}_{J,1} & \cdots & \mathbf{A}_{J,J-1} & \mathbf{A}_{J,J} \end{bmatrix}, \quad \mathbf{B} = \begin{bmatrix} \mathbf{B}_1 \\ \mathbf{B}_2 \\ \vdots \\ \mathbf{B}_J \end{bmatrix}$$

$$\mathbf{C} = \begin{bmatrix} o & \ldots & o & C \end{bmatrix}. \tag{23}$$

Here, $o \in \mathbb{R}^{1\times 5}$ is the zero vector and $C = [0 \;\; 1 \;\; 0 \;\; 0 \;\; 0]$. Note that the lower triangular structure of $\mathbf{A}$ indicates that vehicles in the system only look forward, and the block matrix $\mathbf{A}_{j,i}\,(j > i)$ indicates that the motion of j-th vehicle is affected by the i-th vehicle. This causality reflects direct car following (human-driven vehicles) or V2V connectivity (CAVs).

B. Plant Stability and Head-to-Tail String Stability

To investigate plant stability, we analyze the linearized system (21). Without velocity disturbances on the head vehicle, i.e., $v_0^{\mathrm{amp}} = 0$ in (17, 20) or $U(k) = 0$ in (19), we obtain a linear autonomous map. The local asymptotic stability of the uniform flow equilibrium (11) of system (9) is equivalent to the asymptotic stability of the origin of this map, which is ensured when all the eigenvalues of the matrix $\mathbf{A}$ in (21) are within the unit circle on the complex plane. The eigenvalues $z \in \mathbb{C}$ are given by the characteristic equation

$$\det\left(z\,\mathbf{I} - \mathbf{A}\right) = 0 \tag{24}$$

where $\mathbf{I} \in \mathbb{R}^{5J\times 5J}$ is the identity matrix. A bisection method [30] will be used later to trace the boundaries in the parameter space.

To evaluate head-to-tail string stability, we again use the linearized system (21). With the assumption that the disturbances in the head vehicle's velocity are absolutely integrable and have finite energy, disturbance attenuation can be characterized by the attenuation of sinusoidal perturbations at all frequencies according to Fourier theory and superposition principle. Thus, the head-to-tail string stability condition requires that the amplification ratio from $\tilde{v}_0$ to $\tilde{v}_J$ is always less than 1 at all excitation

frequencies. The amplification ratio can be obtained through transfer functions as explained as follows.

The contributions of the two dependent discrete components $\tilde{v}_0(k)$ and $\tilde{v}_0^{\perp}(k)$ toward the output $\tilde{v}_J(k)$ have to be summed up. Applying Z transform to (21), we can derive the amplification ratio and phase lag as

$$M(\omega) = \left|\Gamma(e^{j\omega\Delta t})\right|, \qquad \psi(\omega) = \angle\Gamma(e^{j\omega\Delta t}) \tag{25}$$

where the head-to-tail transfer function is

$$\Gamma(z) = \mathbf{C}\big(z\mathbf{I} - \mathbf{A}\big)^{-1}\mathbf{B}\mathbf{E} \tag{26}$$

and

$$\mathbf{E} = \begin{bmatrix} 1 & j \end{bmatrix}^{\top} \tag{27}$$

is used to add up the effects of two dependent inputs [30]. Thus, the condition for head-to-tail string stability becomes

$$\sup_{\omega>0} M(\omega) < 1 \tag{28}$$

where M also depends on system parameters. Similar to the plant stability boundaries, the bisection method will be used to trace the string stability boundaries in the parameter space.

Indeed, if the longitudinal controller can be designed for every vehicle, string stability can be achieved. However, in order to mimic scenarios where CCC vehicles are inserted in a chain of human-driven vehicles, we will deliberately set some robots to be string unstable (while responding to the motion of the vehicle immediately ahead). In particular, to mimic the response of human drivers we tune the feedback gains $\alpha_{j,j-1}$ and $\beta_{j,j-1}$ such that, when scaled up to full-sized vehicles, the frequency response matches that of human drivers; see [24] for more details.

V. Results

In this section, we present experimental results with different connectivity topologies to demonstrate effectiveness and flexibility of the controller (5) when the CCC vehicle is operating among string unstable vehicles. We first start with a two-vehicle system and pick a set of parameters to mimic string unstable behaviors of human drivers. Then, we gradually increase the size of vehicle chain such that more "human-driven vehicles" are included. We show that when more "human-driven vehicles" in the chain get connected and more information is incorporated in the controller of the tail CAV, it has more potential to mitigate or eliminate traffic waves. The design rules for connected vehicle systems are gradually built up via experiments of increasing complexity. We note that the sampling time Δt is set to 0.3 [s] to get implementable gains, the integral gains γ_j-s are set to 0.1 [1/s^2], and we use $v_0^* = 0.75$ [m/s]. The other parameters are given in Table II in Section III.

A. Two-Vehicle Experiments

To demonstrate that string stability is achievable when the longitudinal controller can be designed for every vehicle, we first study a predecessor-follower system consisting of two vehicles. Apart from experimentally validating string stable gain

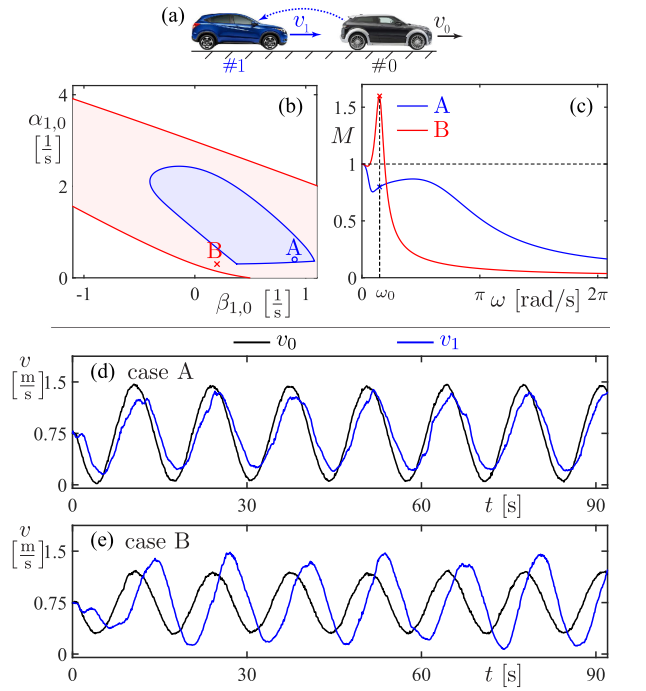

Fig. 4. (a) Two-vehicle configuration. (b) Stability diagram. (c) Frequency response curves for points A and B marked in panel (b). (d) and (e) Experimental velocity profiles when vehicle 0 introduces sinusoidal velocity fluctuations of frequency $\omega_0 = 0.15\,\pi$ [rad/s] for cases A and B, respectively.

combinations, we also conduct experiments to illustrate string unstable behaviors to mimic driving behaviors of humans.

Fig. 4(a) depicts the two-car system where the follower controls its motion based on the predecessor data, while Fig. 4(b) shows the corresponding stability diagram generated based on the conditions in Section IV-B. The red curves and the blue curves represent the plant stability and the string stability boundaries, respectively. The union of red and blue regions indicates the plant stable domain, while the blue shaded region is the string stable domain. The color scheme for stability diagrams is kept the same throughout this paper.

Experiments are conducted on the robots with two sets of gains, that is, $(\alpha_{1,0}\,,\,\beta_{1,0}) = (0.4,\,0.9)$ and $(0.3,\,0.2)$, marked as points A and B in Fig. 4(b). The corresponding frequency response curves (25) are plotted in Fig. 4(c). Case A is string stable for all the frequencies, while case B is string unstable with maximum around $\omega_0 = 0.15\,\pi$ [rad/s]. Fig. 4(d) and (e) show the corresponding experimental velocity profiles when vehicle 0 introduces sinusoidal velocity fluctuations with frequency ω_0. Notice that the fluctuations are attenuated by the follower in case A, but amplified in case B. Similar results can be obtained experimentally for other frequencies, but we choose the frequency ω_0 to emphasize the differences between string stable and string unstable scenarios.

For consistency, we keep the following color coding for vehicles in different configurations in the paper. Black indicates the head vehicle introducing velocity fluctuations, red vehicles represent string unstable vehicles configured the same way as

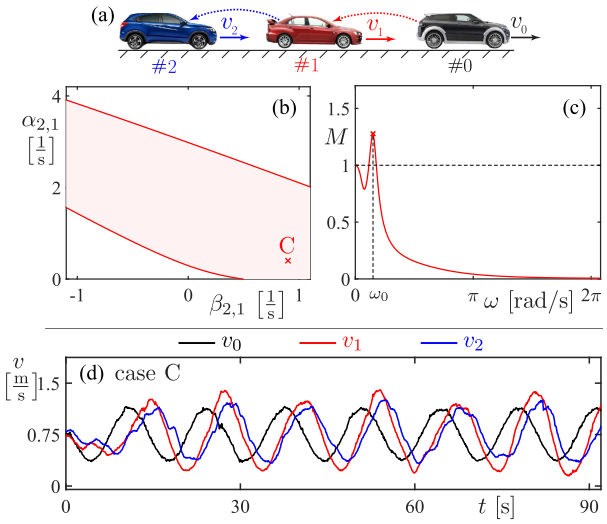

Fig. 5. (a) Three-vehicle configuration. (b) Stability diagram. (c) Frequency response curve for point C marked in panel (b). (d) Experimental velocity profiles for case C when vehicle 0 introduces sinusoidal velocity fluctuations at $\omega_0 = 0.15\,\pi$ [rad/s].

case B in Fig. 4, and blue represents CCC vehicles with gain parameters to be designed. We recall that case B is used to mimic string unstable behaviors of human-driven vehicles; see [24]. As pointed out in Section II, different vehicles may have different parameters, but in the following we use same parameters for string unstable vehicles to represent worst case scenario in term of string instability.

B. Three-Vehicle Experiments

Here, we use three vehicles to demonstrate that in the presence of string unstable vehicles, it may not be possible to ensure head-to-tail string stability when the CCC vehicle only utilizes motion information of its immediate predecessor, but this goal can be achieved when CCC vehicle utilizes information from two vehicles ahead (the second one being beyond the line of sight).

Fig. 5(a) shows a chain of three vehicles where the following vehicles only rely on their own direct predecessor for longitudinal control. Vehicle 1 is a string unstable vehicle with gains used for case B in Fig. 4. The stability diagram in Fig. 5(b) indicates that the system cannot achieve head-to-tail string stability whatever gains are selected for vehicle 3 with controller (5). To demonstrate this behavior we marked point C at $(\alpha_{2,1}\,,\,\beta_{2,1}) = (0.4,\,0.9)$ in Fig. 5(b), that is, vehicle 2 is configured the same way as case A in Fig. 4, i.e., it is 1-to-2 string stable. However as shown by the (head-to-tail) frequency response in Fig. 5(c), the overall system is head-to-tail string unstable. The experimental velocity profiles are shown in Fig. 5(d) at frequency ω_0. Observe that the velocity fluctuations of vehicle 1 are attenuated slightly by vehicle 2. However, the fluctuations of vehicle 2 are still greater than those of vehicle 0.

To improve the performance, the CCC vehicle can take advantage of V2X communication and utilize the information of the two predecessors; see Fig. 6(a). For the other communication

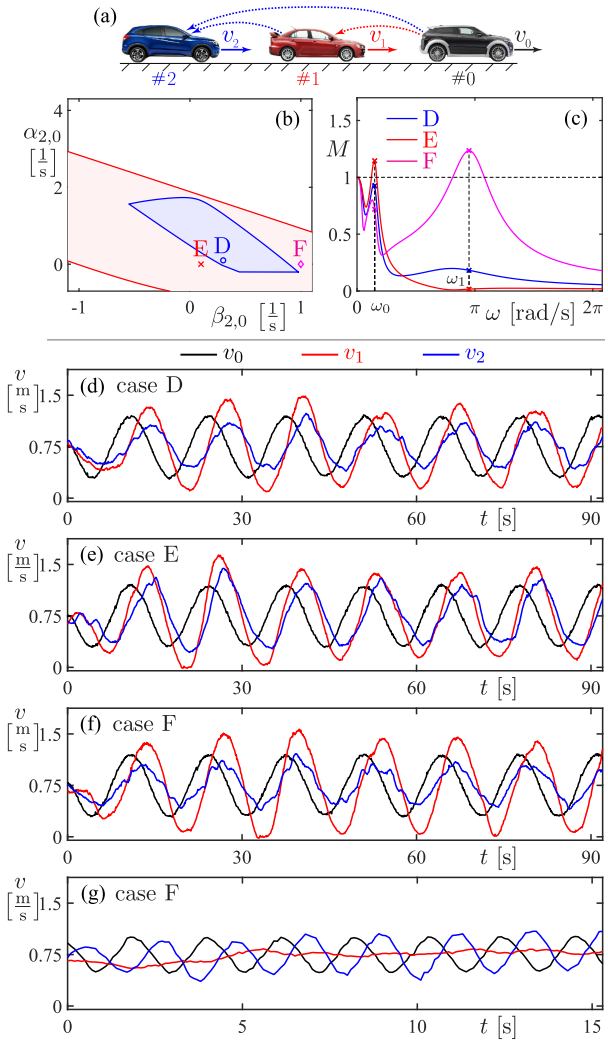

Fig. 6. (a) Three-vehicle configuration. (b) Stability diagram. (c) Frequency response curves for points D, E, and F marked in panel (b). (d) and (e) Experimental velocity profiles for cases D and E when vehicle 0 introduces sinusoidal velocity fluctuations at $\omega_0 = 0.15\,\pi$ [rad/s]. (f) and (g) Experimental velocity profiles for case F when vehicle 0 introduces sinusoidal velocity fluctuations at $\omega_0 = 0.15\,\pi$ [rad/s] and $\omega_1 = 0.95\,\pi$ [rad/s], respectively.

links, the control gains are kept the same as case C in Fig. 5. The stability diagram in Fig. 6(b) is plotted in the plane of the control gains between vehicles 0 and 2. It can be seen that with appropriately chosen parameters for this extra link the overall system can achieve head-to-tail string stability. In Fig. 6(b), the points D, E, and F mark the gain combinations $(\alpha_{2,0}\,,\,\beta_{2,0}) = (0.1,\,0.3)$, $(0,\,0.1)$, and $(0,\,1)$. The corresponding (head-to-tail) frequency responses shown in Fig. 6(c) indicate that case D is head-to-tail string stable, while cases E and F are head-to-tail string unstable with critical frequencies around $\omega_0 = 0.15\,\pi$ [rad/s] and $\omega_1 = 0.95\,\pi$ [rad/s], respectively.

Experiments are conducted for cases D and E using sinusoidal velocity fluctuations for vehicle 0 at frequency ω_0. The resulting velocity profiles shown in Fig. 6(d) and (e) indicate that vehicle 2 can make the fluctuations smaller than those of vehicle 0 in case D, but cannot achieve such disturbance attenuation in

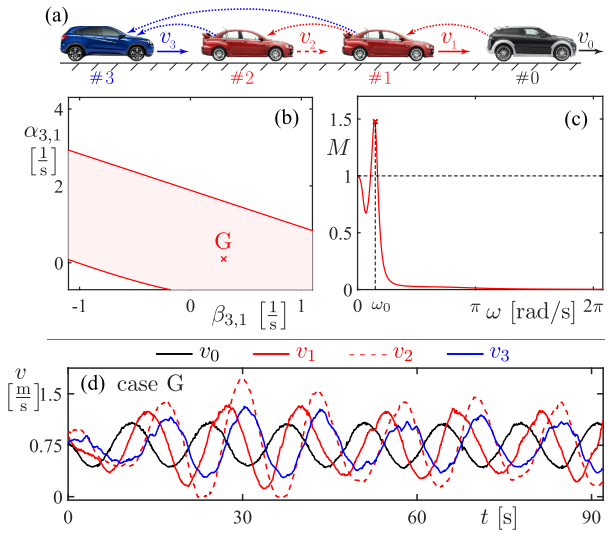

Fig. 7. (a) Four-vehicle configuration. (b) Stability diagram. (c) Frequency response curve for point G marked in panel (b). (d) Experimental velocity profiles when vehicle 0 introduces sinusoidal velocity fluctuations at frequency $\omega_0 = 0.15\,\pi$ [rad/s].

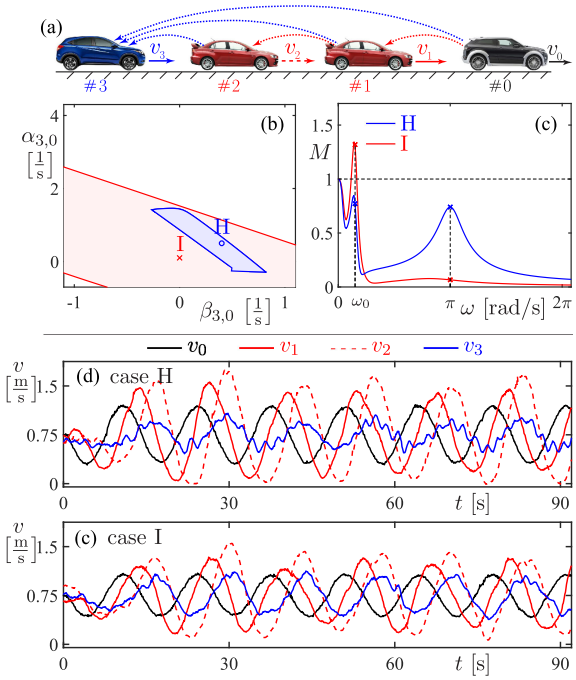

Fig. 8. (a) Four-vehicle configuration. (b) Stability diagram. (c) Frequency response curves for points H and I marked in panel (b). (d) and (e) Experimental velocity profiles when vehicle 0 introduces sinusoidal velocity fluctuations at frequency $\omega_0 = 0.15\,\pi$ [rad/s].

case E. Experiments for case F show a scenario where vehicle 2 attenuates the fluctuations of vehicle 0 at ω_0 but amplifies the fluctuations at ω_1 even though vehicle 1 attenuate those, as shown in Fig. 6(f) and (g). Case F is indeed head-to-tail string unstable due to amplifying high-frequency signals. This emphasizes that CCC must be appropriately designed; otherwise, unexpected oscillations may impair system performance.

C. Four-Vehicle Experiments

In this section, we incorporate more string unstable vehicles into the system and show that it is beneficial to utilize more beyond-line-of-sight information in CCC design. We also demonstrate that the resulting connectivity topology has some level of flexibility to tolerate the absence of certain communication links.

Fig. 7(a) delineates a scenario that includes two string unstable vehicles with gains corresponding to case B in Fig. 4, while the CCC vehicle at the tail relies on the motion of its two immediate predecessors while using the same gains as in Fig. 6(a), i.e., $(\alpha_{3,2}\,,\,\beta_{3,2}) = (0.4,\,0.9)$. The stability diagram in Fig. 7(b), plotted in the plane of control gains between vehicles 1 and 3, shows that head-to-tail string stability is not achievable. We choose the set of gains $(\alpha_{3,1}\,,\,\beta_{3,1}) = (0.1,\,0.3)$, corresponding to point G in Fig. 7(b), so that the subsystem consisting vehicles 1–3 is equivalent to the system for case D in Fig. 6. The corresponding (head-to-tail) frequency response in Fig. 7(c) indicates head-to-tail string instability with maximum around $\omega_0 = 0.15\,\pi$ [rad/s], and the experimental velocity profiles at this frequency are shown in Fig. 7(d). It can be observed that the fluctuations of vehicle 0 are amplified by vehicles 1 and 2, but then attenuated by vehicle 3. However, the amplitude of the fluctuations for vehicle 3 is between the amplitudes of vehicles 0 and 1. This means that the subsystem consisting of vehicles 1–3 is 1-to-3 string stable, whereas the overall system is head-to-tail string unstable.

To improve the performance, we consider a scenario where the information from all three predecessors is utilized by the CCC vehicle 3, as shown in Fig. 8(a). The control gains are kept the same as those for case G in Fig. 7 for all the communication links. Fig. 8(b) shows the stability diagram in the plane of control gains between vehicles 0 and 3, indicating that the overall system can achieve head-to-tail string stability with appropriate gains for the additional link. Two points are marked H and I in Fig. 8(b) at $(\alpha_{3,0}\,,\,\beta_{3,0}) = (0.5,\,0.4)$ and $(0,\,0.1)$ and the (head-to-tail) frequency response curves in Fig. 8(c) show that in case H one can achieve head-to-tail string stability, but this is not true in case I. The experimental velocity profiles for case H are shown in Fig. 8(d), indicating that the amplitude of the fluctuations of vehicle 3 is less than that of vehicle 0, and noticeable fluctuations around π [rad/s] also arise in vehicle 3 in correspondence with the extra peak in Fig. 8(c). On the other hand, the experimental result shown in Fig. 8(e) for case I reveals vehicle 3 still amplifies the velocity fluctuations of vehicle 0 if the gains are not chosen properly.

Finally, we test a scenario where the motion information from some vehicles are not available (which is the case when having human-driven vehicles that are not equipped with V2X devices). Fig. 9(a) shows a scenario similar to the one in Fig. 8(a) except the lack of communication link between vehicles 1 and 3, while all the control gains are kept unchanged. The stability diagram in Fig. 9(b) is plotted in the plane of control gains for the link between vehicles 0 and 3, indicating that head-to-tail string stability is still achievable without this link. The (head-to-tail)

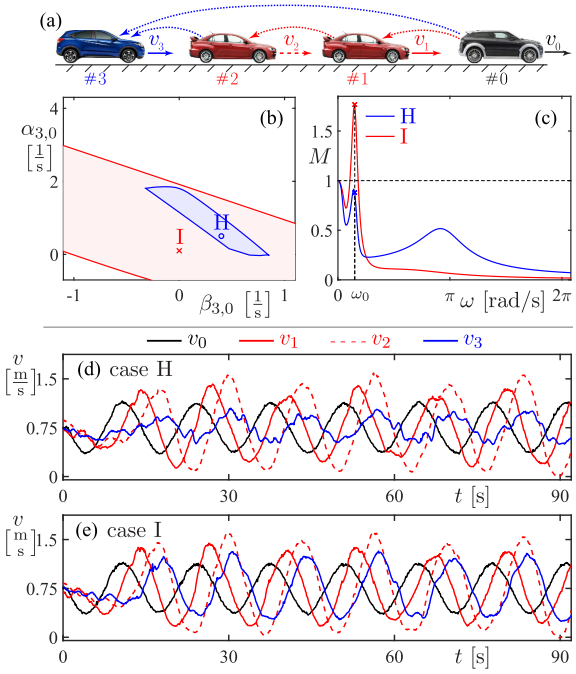

Fig. 9. (a) Four-vehicle configuration. (b) Stability diagram. (c) Frequency response curves for points H and I marked in panel (b). (d) and (e) Experimental velocity profiles when vehicle 0 introduces sinusoidal velocity fluctuations at frequency $\omega_0 = 0.15\,\pi$ [rad/s].

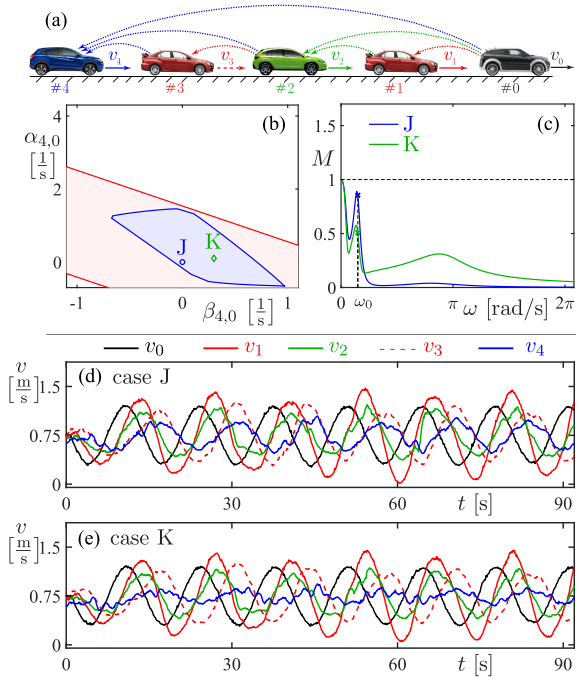

Fig. 10. (a) Five-vehicle configuration. (b) Stability diagram. (c) Frequency response curves for points J and K marked in panel (b). (d) and (e) Experimental velocity profiles when vehicle 0 introduces sinusoidal velocity fluctuations at frequency $\omega_0 = 0.15\,\pi$ [rad/s].

frequency response curves corresponding to the points marked H and I are shown in Fig. 9(b). Observe that, despite the missing link, in case H head-to-tail string stability is still maintained apart from a slight increase in the amplification ratio around ω_0, while case I is indeed still head-to-tail string unstable. The velocity profiles in Fig. 9(d) and (e) are consistent with the theoretical results.

D. Five-Vehicle Experiments

Here, we study whether the performance can be further improved by including multiple CCC vehicles. Fig. 10(a) shows a cascaded configuration of two identical systems used in Fig. 6, except the addition of an extra communication link between vehicles 0 and 4. The red vehicles still represent string unstable vehicles as discussed in Section V-A, while the blue and green vehicles use the control scheme on their two direct predecessors according to case D in Fig. 6. The stability diagram in Fig. 10(b) is plotted in the plane of the control gains of the longest link, and the points marked J and K correspond to $(\alpha_{4,0}\,,\,\beta_{4,0}) = (0,\,0)$ and $(0.1,\,0.3)$. The corresponding (head-to-tail) frequency response curves shown in Fig. 10(c) indicate that both cases are head-to-tail string stable but the amplification ratio at frequency ω_0 is smaller in case K.

The velocity profiles are shown in Fig. 10(d) and (e). In case J where the extra long link is not utilized, the amplified fluctuations in vehicle 1 are first attenuated by vehicle 2, then amplified by vehicle 3, and finally attenuated again when reaching vehicle 4. Similar behaviors can be observed from Fig. 10(e) for the experiment in case K except that vehicle 4 has smaller fluctuations than those in Fig. 10(d) for case J.

In this section, we investigated scenarios that a CAV has the potential to ensure head-to-tail string stability if the vehicles ahead are equipped with communication devices. Note that this head-to-tail string stability guarantee is based on the known information of all preceding vehicles. If these parameters are not known exactly, we might not be able to achieve head-to-tail string stability, but we can still damp down the disturbance with properly designed controller for CAVs (see Fig. 7). That is, even when the penetration rate of CAVs is low, traffic waves can be mitigated, and when the penetration rate is high, phantom traffic jams can be eliminated.

VI. Conclusion

In this paper, we proposed a class of longitudinal controllers for CAVs that allows us to exploit information from multiple connected vehicles ahead using V2X communication. The control algorithms were designed by using mathematical models representing the continuous time vehicle dynamics subject to digital control. The theoretical results about plant stability and string stability were summarized using stability diagrams. A scaled connected vehicle testbed consisting ground robots capable of wireless peer-to-peer communication was used to realize the developed connected cruise control algorithms experimentally.

Through a sequence of experiments, we demonstrated that CAV may significantly benefit smoothness of human-dominated traffic by attenuating velocity perturbations that are typically amplified by human drivers. We found that, while limited improvements can be achieved by AVs (without connectivity), utilizing beyond-line-of-sight information provided by V2X

connectivity significantly enhances the impact of automation. By utilizing our model-based design, adding more connectivity can lead to more benefits in terms of mitigating velocity fluctuations while remaining robust against loss of communication links. Finally, the proposed design remains scalable as penetration of CAVs increases, making real-world deployment feasible.

Future research will include searching for optimal parameter combinations that ensure safety of CCC algorithms as well as experiments with full size vehicles.

APPENDIX

A. Derivation of the Dynamic Model

Equations (13)–(15) can be solved backward sequentially. Induction of (15) gives

$$\tilde{\varepsilon}_j(k+1) = \frac{\Delta t}{t_j^{\mathrm{h}}}\,\tilde{h}_j(k) - \Delta t\,\tilde{v}_j(k) + \tilde{\varepsilon}_j(k) \tag{29}$$

while integration of (14) yields

$$\tilde{v}_j(t) = \mathrm{e}^{-c(t-t_k)}\left(\tilde{v}_j(k) - \frac{\tilde{u}_j}{c}\right) + \frac{\tilde{u}_j}{c} \tag{30}$$

for $j = 1\,,\,\ldots\,,\,J$, where

$$\tilde{u}_j = \sum_{i=0}^{j-1}\left[\frac{\alpha_{j,\,i}}{t_j^{\mathrm{h}}}\cdot\frac{1}{j-i}\sum_{l=i+1}^{j}\tilde{h}_l(k-1) + \beta_{j,\,i}\,\tilde{v}_i(k-1)\right.$$
$$\left.-(\alpha_{j,\,i}+\beta_{j,\,i})\,\tilde{v}_j(k-1)\right] + \gamma_j\,\tilde{\varepsilon}_j(k)\,. \tag{31}$$

Substituting (17), (30) into (13) and then integrating both sides with initial condition, we obtain

$$\tilde{h}_1(t) = \tilde{h}_1(k) - \frac{v_0^{\mathrm{amp}}}{\omega}\big(\cos(\omega\,t) - \cos(\omega\,t_k)\big)$$
$$+\frac{\mathrm{e}^{-c(t-t_k)}-1}{c}\left(\tilde{v}_1(k) - \frac{\tilde{u}_1}{c}\right) - \frac{\tilde{u}_1}{c}(t-t_k) \tag{32}$$

and

$$\tilde{h}_j(t) = \tilde{h}_j(t_k) + \frac{\tilde{u}_{j-1}-\tilde{u}_j}{c}(t-t_k)$$
$$-\frac{\mathrm{e}^{-c(t-t_k)}-1}{c}\left(\tilde{v}_{j-1}(k) - \tilde{v}_j(k) - \frac{\tilde{u}_{j-1}-\tilde{u}_j}{c}\right) \tag{33}$$

for $j = 2\,,\,\ldots\,,\,J$.

Evaluating (32), (33), (30) at instant $t = t_{k+1}$ gives

$$\tilde{h}_1(k+1) = \tilde{h}_1(k) - \theta_1\tilde{v}_1(k) + \theta_2 v_0^{\mathrm{amp}}\sin(k\,\omega\,\Delta t)$$
$$+\theta_3 v_0^{\mathrm{amp}}\cos(k\omega\Delta t) - \theta_4\tilde{u}_1 \tag{34}$$

$$\tilde{h}_j(k+1) = \tilde{h}_j(k) - \theta_1\tilde{v}_j(k) + \theta_1\tilde{v}_{j-1}(k)$$
$$+\theta_4\,(\tilde{u}_{j-1}-\tilde{u}_j)\;,j = 2\,,\,\ldots\,,\,J \tag{35}$$

and

$$\tilde{v}_j(k+1) = \mathrm{e}^{-c\Delta t}\tilde{v}_j(k) + \theta_1\tilde{u}_j \tag{36}$$

for $j = 1\,,\,\ldots\,,\,J$, where

$$\theta_1 = \frac{1-\mathrm{e}^{-c\Delta t}}{c}\,,\qquad \theta_2 = \frac{\sin(\omega\,\Delta t)}{\omega}$$
$$\theta_3 = \frac{1-\cos(\omega\,\Delta t)}{\omega}\,,\qquad \theta_4 = \frac{\mathrm{e}^{-c\Delta t}-1+c\Delta t}{c^2}\,. \tag{37}$$

Through the use of (20), (31), and algebraic manipulations, (29), (34), (35), and (36) can be simplified and then combined into the model (18) with

$$\mathbf{A}_{j,\,j} = \begin{bmatrix} 1 & -\theta_1 & -\gamma_j\theta_4 & -\xi_{j,\,j-1}\theta_4 & \overline{\kappa}_j^{\mathrm{s}}\theta_4 \\ 0 & \mathrm{e}^{-c\Delta t} & \gamma_j\theta_1 & \xi_{j,\,j-1}\theta_1 & -\overline{\kappa}_j^{\mathrm{s}}\theta_1 \\ \frac{\Delta t}{t_j^{\mathrm{h}}} & -\Delta t & 1 & 0 & 0 \\ 1 & 0 & 0 & 0 & 0 \\ 0 & 1 & 0 & 0 & 0 \end{bmatrix} \tag{38}$$

for $j = 1\,,\,\ldots\,,\,J$,

$$\mathbf{A}_{j,\,j-1} = \begin{bmatrix} 0 & \theta_1 & \gamma_{j-1}\theta_4 & \widehat{\xi}_{j,\,j-2}\theta_4 & -\zeta_j\theta_4 \\ 0 & 0 & 0 & \xi_{j,\,j-2}\theta_1 & \beta_{j,\,j-1}\theta_1 \\ 0 & 0 & 0 & 0 & 0 \\ 0 & 0 & 0 & 0 & 0 \\ 0 & 0 & 0 & 0 & 0 \end{bmatrix}$$

$$\mathbf{B}_j = \begin{bmatrix} \widehat{\beta}_{j,\,0}\theta_4\cos(\omega\,\Delta t) & -\widehat{\beta}_{j,\,0}\theta_4\sin(\omega\,\Delta t) \\ \beta_{j,\,0}\theta_1\cos(\omega\,\Delta t) & -\beta_{j,\,0}\theta_1\sin(\omega\,\Delta t) \\ 0 & 0 \\ 0 & 0 \\ 0 & 0 \end{bmatrix} \tag{39}$$

for $j = 2\,,\,\ldots\,,\,J$,

$$\mathbf{A}_{j,\,l} = \begin{bmatrix} 0 & 0 & 0 & \widehat{\xi}_{j,\,l-1}\theta_4 & \widehat{\beta}_{j,\,l}\theta_4 \\ 0 & 0 & 0 & \xi_{j,\,l-1}\theta_1 & \beta_{j,\,l}\theta_1 \\ 0 & 0 & 0 & 0 & 0 \\ 0 & 0 & 0 & 0 & 0 \\ 0 & 0 & 0 & 0 & 0 \end{bmatrix} \tag{40}$$

for $j = 3\,,\,\ldots\,,\,J\,,\;l = 1\,,\,\ldots\,,\,j-2$, and

$$\mathbf{B}_1 = \begin{bmatrix} \theta_2 - \beta_{1,0}\theta_4\cos(\omega\Delta t) & \theta_3 + \beta_{1,0}\theta_4\sin(\omega\Delta t) \\ \beta_{1,0}\theta_1\cos(\omega\Delta t) & -\beta_{1,0}\theta_1\sin(\omega\Delta t) \\ 0 & 0 \\ 0 & 0 \\ 0 & 0 \end{bmatrix} \tag{41}$$

where

$$\xi_{r,l} = \frac{1}{t_r^{\rm h}} \sum_{i=0}^{l} \frac{\alpha_{r,i}}{r-i}\,, \qquad \overline{\kappa}_r^{\rm s} = \sum_{i=0}^{r-1} (\alpha_{r,i} + \beta_{r,i})$$
$$\widehat{\xi}_{r,l} = \xi_{r-1,l} - \xi_{r,l}\,, \qquad \widehat{\beta}_{r,l} = \beta_{r-1,\,l} - \beta_{r,\,l}$$
$$\zeta_r = \overline{\kappa}_{r-1}^{\rm s} + \beta_{r,r-1}\,. \tag{42}$$

B. Similarity Verification

In this section, we apply similitude theory and find all the dimensionless quantities according to Buckingham Π theorem [31]. Then, we verify that all these quantities are equal for the scaled robots and real vehicles to ensure our method are scalable. According to Newton's law, both the robot and real vehicles are governed by (7) in the longitudinal direction when assumptions in Section IV hold. The general relationship of the variables is

$$f(h_j,\, v_j,\, \dot{h}_j,\, \dot{v}_j,\, v_{j-1},\, u_j) = 0 \tag{43}$$

which includes two primary dimensions, i.e., length $[L]$ and time $[T]$, where $[\cdot]$ denotes "the dimension of." According to Buckingham Π theorem, we choose h_j and v_j as repeating variables, and can obtain the other dimensionless Π groups as

$$\Pi_1 = \frac{\dot{h}_j}{v_j}\,,\ \Pi_2 = \frac{\dot{v}_j\, h_j}{v_j^2}\,,\ \Pi_3 = \frac{v_{j-1}}{v_j}\,,\ \Pi_4 = \frac{u_j\, h_j}{v_j^2}\,. \tag{44}$$

Thus, the final relationship is of the form

$$f(\Pi_1,\, \Pi_2,\, \Pi_3,\, \Pi_4) = 0\,. \tag{45}$$

Based on Table I, we can see that each Π group is equal for the scaled robots and real vehicles. We remark that Buckingham Π theorem also holds for the closed-loop system when controller (5) is included. Thus, two systems are similar.

ACKNOWLEDGMENT

The authors would like to thank all the members involved in the Connected Ground Robot Experiment (CGRE) Project.

REFERENCES

[1] D. Schrank, B. Eisele, T. Lomax, and J. Bak, "2015 urban mobility scorecard," Texas A&M Transportation Institute, College Station, TX, USA, Tech. Rep., 2015.

[2] A. Festag, "Standards for vehicular communication—From IEEE 802.11p to 5G," *Elektrotechnik Informationstechnik*, vol. 132, no. 7, pp. 409–416, 2015.

[3] J. B. Kenney, "Dedicated short-range communications (DSRC) standards in the United States," *Proc. IEEE*, vol. 99, no. 7, pp. 1162–1182, Jul. 2011.

[4] *Dedicated Short Range Communications (DSRC) Message Set Dictionary*, SAE International, Warrendale, PA, USA, Standard J2735, 2016.

[5] A. Bazzi, B. M. Masini, A. Zanella, and I. Thibault, "On the performance of IEEE 802.11p and LTE-V2V for the cooperative awareness of connected vehicles," *IEEE Trans. Veh. Technol.*, vol. 66, no. 11, pp. 10 419–10 432, Nov. 2017.

[6] E. Uhlemann, "Time for autonomous vehicles to connect [connected vehicles]," *IEEE Veh. Technol. Mag.*, vol. 13, no. 3, pp. 10–13, Sep. 2018.

[7] S. Darbha, S. Konduri, and P. R. Pagilla, "Benefits of V2V communication for autonomous and connected vehicles," *IEEE Trans. Intell. Transp. Syst.*, vol. 20, no. 5, pp. 1954–1963, May 2019.

[8] B. van Arem, C. J. G. van Driel, and R. Visser, "The impact of cooperative adaptive cruise control on traffic-flow characteristics," *IEEE Trans. Intell. Transp. Syst.*, vol. 7, no. 4, pp. 429–436, Dec. 2006.

[9] V. Milanes, J. Alonso, L. Bouraoui, and J. Ploeg, "Cooperative maneuvering in close environments among cybercars and dual-mode cars," *IEEE Trans. Intell. Transp. Syst.*, vol. 12, no. 1, pp. 15–24, Mar. 2011.

[10] J. Ploeg, E. Semsar-Kazerooni, G. Lijster, N. van de Wouw, and H. Nijmeijer, "Graceful degradation of cooperative adaptive cruise control," *IEEE Trans. Intell. Transp. Syst.*, vol. 16, no. 1, pp. 488–497, Feb. 2015.

[11] M. di Bernardo, A. Salvi, and S. Santini, "Distributed consensus strategy for platooning of vehicles in the presence of time varying heterogeneous communication delays," *IEEE Trans. Intell. Transp. Syst.*, vol. 16, no. 1, pp. 102–112, Feb. 2015.

[12] S. E. Shladover, C. Nowakowski, X.-Y. Lu, and R. Ferlis, "Cooperative adaptive cruise control definitions and operating concepts," *Transp. Res. Rec.: J. Transp. Res. Board*, vol. 2489, pp. 145–152, 2015.

[13] K. C. Dey *et al.*, "A review of communication, driver characteristics, and controls aspects of cooperative adaptive cruise control (CACC)," *IEEE Trans. Intell. Transp. Syst.*, vol. 17, no. 2, pp. 491–509, Feb. 2016.

[14] Y. Li, C. Tang, S. Peeta, and Y. Wang, "Nonlinear consensus-based connected vehicle platoon control incorporating car-following interactions and heterogeneous time delays," *IEEE Trans. Intell. Transp. Syst.*, vol. 20, no. 6, pp. 2209–2219, Jun. 2019.

[15] Y. Zheng, S. E. Li, K. Li, and W. Ren, "Platooning of connected vehicles with undirected topologies: Robustness analysis and distributed H-infinity controller synthesis," *IEEE Trans. Intell. Transp. Syst.*, vol. 19, no. 5, pp. 1353–1364, May 2018.

[16] Z. Chen and B. B. Park, "Preceding vehicle identification for cooperative adaptive cruise control platoon forming," *IEEE Trans. Intell. Transp. Syst.*, to be published.

[17] V. Turri, B. Besselink, and K. H. Johansson, "Cooperative look-ahead control for fuel-efficient and safe heavy-duty vehicle platooning," *IEEE Trans. Control Syst. Technol.*, vol. 25, no. 1, pp. 12–28, Jan. 2017.

[18] X.-Y. Lu and S. Shladover, "Integrated ACC and CACC development for heavy-duty truck partial automation," in *Proc. Amer. Control Conf.*, 2017, pp. 4938–4945.

[19] G. Orosz, J. I. Ge, C. R. He, S. S. Avedisov, W. B. Qin, and L. Zhang, "Seeing beyond the line of sight – controlling connected automated vehicles," *ASME Dyn. Syst. Control Mag.*, vol. 5, no. 4, pp. 8–12, 2017.

[20] S. S. Avedisov and G. Orosz, "Nonlinear network modes in cyclic systems with applications to connected vehicles," *J. Nonlinear Sci.*, vol. 25, no. 4, pp. 1015–1049, 2015.

[21] W. B. Qin and G. Orosz, "Scalable stability analysis on large connected vehicle systems subject to stochastic communication delays," *Transp. Res. Part C*, vol. 83, pp. 39–60, 2017.

[22] L. Zhang and G. Orosz, "Consensus and disturbance attenuation in multi-agent chains with nonlinear control and time delays," *Int. J. Robust Nonlinear Control*, vol. 27, no. 5, pp. 781–803, 2017.

[23] J. I. Ge and G. Orosz, "Optimal control of connected vehicle systems with communication delay and driver reaction time," *IEEE Trans. Intell. Transp. Syst.*, vol. 18, no. 8, pp. 2056–2070, Aug. 2017.

[24] W. B. Qin and G. Orosz, "Experimental validation of string stability for connected vehicles subject to information delay," *IEEE Trans. Control Syst. Technol.*, to be published.

[25] L. Zhang and G. Orosz, "Motif-based design for connected vehicle systems in presence of heterogeneous connectivity structures and time delays," *IEEE Trans. Intell. Transp. Syst.*, vol. 17, no. 6, pp. 1638–1651, Jun. 2016.

[26] Y. Zheng, S. E. Li, K. Li, and L. Y. Wang, "Stability margin improvement of vehicular platoon considering undirected topology and asymmetric control," *IEEE Trans. Control Syst. Technol.*, vol. 24, no. 4, pp. 1253–1265, Jul. 2016.

[27] B. Besselink and K. H. Johansson, "String stability and a delay-based spacing policy for vehicle platoons subject to disturbances," *IEEE Trans. Autom. Control*, vol. 62, no. 9, pp. 4376–4391, Sep. 2017.

[28] G. Rödönyi, "An adaptive spacing policy guaranteeing string stability in multi-brand ad hoc platoons," *IEEE Trans. Intell. Transp. Syst.*, vol. 19, no. 6, pp. 1902–1912, Jun. 2018.

[29] S. Öncü, N. van de Wouw, and H. Nijmeijer, "Cooperative adaptive cruise control: Tradeoffs between control and network specifications," in *Proc. 14th Int. IEEE Conf. Intell. Transp. Syst.*, 2011, pp. 2051–2056.

[30] W. B. Qin, M. M. Gomez, and G. Orosz, "Stability and frequency response under stochastic communication delays with applications to connected cruise control design," *IEEE Trans. Intell. Transp. Syst.*, vol. 18, no. 2, pp. 388–403, Feb. 2017.

[31] G. I. Barenblatt, *Scaling, Self-Similarity, and Intermediate Asymptotics: Dimensional Analysis and Intermediate Asymptotics*. Cambridge, U.K.: Cambridge Univ. Press, 1996.

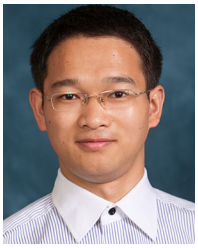

Wubing B. Qin received the B.Eng. degree in mechanical science and engineering from the School of Mechanical Science and Engineering, Huazhong University of Science and Technology, Wuhan, China, in 2011, and the M.Sc. and Ph.D. degree in mechanical engineering from the University of Michigan, Ann Arbor, MI, USA, in 2016 and 2018, respectively.

In 2018, he joined Aptiv, Michigan, USA, where he is currently an ADAS algorithm developer. His research focuses on dynamics and control of connected vehicles, digital systems, ground robotics, and nonlinear and stochastic systems with time delays.

Gábor Orosz received the M.Sc. degree in engineering physics from the Budapest University of Technology, Budapest, Hungary, in 2002 and the Ph.D. degree in engineering mathematics from the University of Bristol, U.K. in 2006.

He held Postdoctoral positions with the University of Exeter, U.K., and with the University of California, Santa Barbara, CA, USA. In 2010, he joined the University of Michigan, Ann Arbor, MI, USA, where he is currently an Associate Professor in Mechanical Engineering. His research focuses on nonlinear dynamics and control, time delay systems, networks and complex systems with applications on connected automated vehicles and biological networks.